

# Implementation of non-local arbitrary two-qubit controlled gates via geometric quantum computation with Rydberg anti-blockade

Le-Jiang Yu, Jia Zheng, and Kun Pu

*Department of Physics, Zhejiang Normal University, Jinhua 321004, China*

Chao Gao\*

*Department of Physics, Zhejiang Normal University, Jinhua 321004, China*

*Zhejiang Institute of Photoelectronics, Jinhua 321004, China and*

*Key Laboratory of Optical Information Detection and Display Technology of Zhejiang,*

*Zhejiang Normal University, Jinhua, 321004, China*

In the context of Rydberg anti-blockade, this paper proposes a new scheme for a high-fidelity controlled-unitary gate based on non-adiabatic holonomic quantum computation. Under specific detuning and interaction conditions, the scheme achieves a suitable evolution path for non-adiabatic holonomic quantum computation through reverse engineering of pulse parameters. Numerical simulations show that the geometric gate maintains high fidelity even in the presence of spontaneous radiation and laser intensity errors. Finally, we extend our designed quantum gates to non-local gates and investigate their use in converting four-qubit entangled states. This finding indicates the potential applicability of our scheme to complex quantum information processing tasks.

## I. INTRODUCTION

The field of quantum information merges quantum mechanics and information science, demonstrating immense potential in accelerating complex problem-solving, ensuring secure information transmission, and achieving high-precision detection [1]. Among its branches, quantum computing has already broken through fundamental limitations of classical computing in certain specific areas, showcasing significant application prospects [2–5]. The key to realizing quantum computing, however, hinges on the precise manipulation of quantum logic gates, which directly determines the execution efficiency and computational power of quantum algorithms. Currently, achieving high-fidelity, scalable quantum gate operations across different physical platforms has become a core challenge in advancing the practical application of quantum computing.

The design of quantum logic gate schemes must meet sufficiently high fidelity and robustness requirements. Geometric quantum computation (GQC), utilizing geometric phases that depend only on evolution paths rather than dynamical details, inherently provides robustness against local noise [3, 6–8]. While early adiabatic approaches required long evolution times that increased susceptibility to decoherence, the development of non-adiabatic holonomic quantum computation (NHQC) overcame these adiabatic limitations [9–14]. However, NHQC still needs to satisfy two conditions: (i) the cyclic evolution condition and (ii) the parallel transport condition [15]. Currently, researchers have conducted extensive studies on NHQC-based quantum gate schemes across different physical platforms such as superconducting circuits [16], NV centers [17], and nuclear magnetic resonance [18], gradually relaxing the restrictions of non-adiabatic holonomic conditions [19–21]. Among them, the NHQC+ scheme, in which condition (ii) is relaxed to only require the accumulated dynamic phase throughout the entire process to be zero, has been widely applied [22].

Currently, Rydberg atom platforms have emerged as a highly promising system in the field of quantum information processing, offering unique advantages such as strongly tunable interactions, long coherence times, and high-fidelity quantum operations [23]. Leveraging the dipole-dipole interactions between Rydberg atoms, the Rydberg blockade effect suppresses simultaneous excitation of nearby atoms, providing a reliable scheme for constructing high-fidelity two-qubit quantum logic gates, which have been widely applied in quantum computing and simulation [24–27]. However, this mechanism has significant limitations: strict spatial constraints require interatomic distances to be smaller than the blockade radius, leading to notable crosstalk between qubits at micrometer-scale interaction distances. Increasing the distance by raising the principal quantum number introduces additional complications. Moreover, implementing multi-qubit gates using the blockade effect demands complex timing control [28]. These shortcomings have motivated the pursuit of different interaction regimes, with the Rydberg anti-blockade effect standing out as a robust and versatile candidate.

The Rydberg anti-blockade effect enables simultaneous excitation of multiple atoms into Rydberg states. Experimentally, by adjusting the detuning between the laser frequency and atomic transition frequency, resonant transitions

---

\* gaochao@zjnu.edu.cn

can be achieved when specific conditions are met through compensation of the energy shifts induced by Rydberg interactions [29]. Current NHQC-based two-qubit gate schemes, utilizing the anti-blockade effect, primarily focus on SWAP gates [15, 30–32], while successful implementations of arbitrary controlled-unitary (CU) gates remain scarce.

In this work, we explore the implementation of a two-qubit CU gate using the anti-blockade mechanism and incorporate NHQC+ dynamics into our scheme. For pulse design, we employ an inverse engineering approach based on dynamical invariants. We then numerically verify the robustness of the scheme. Lastly, by extending the scheme to non-local quantum gates, we discuss its potential value for applications.

## II. RYDBERG ANTIBLOCKADE CU GATE BASED ON NHQC+ DYNAMICS

### A. Model and realization of the gates

Now we demonstrate how to construct a two-qubit CU gate using NHQC+ dynamics. In our scheme, there are two Rydberg atoms, each consisting of three energy levels: two ground states  $|0\rangle$ ,  $|1\rangle$ , and a Rydberg state  $|r\rangle$  (as shown in Fig. 1). For atom 1, the  $|0\rangle$  state remains idle, and the transition  $|1\rangle_1 \leftrightarrow |r\rangle_1$  is driven by a laser with Rabi frequency  $\Omega_{11}$  and blue detuning  $\Delta_1$ . For atom 2, the  $|0\rangle$  and  $|1\rangle$  states are coupled to  $|r\rangle$  with Rabi frequencies  $\Omega_{21}$  and  $\Omega_{22}$ , respectively, and with the same detuning  $\Delta_2$ . Under the interaction picture, the Hamiltonian of the system can be written as

$$\hat{H} = \hat{H}_1 + \hat{H}_2 + \hat{V}_{rr}, \quad (1)$$

where  $\hat{H}_1$  and  $\hat{H}_2$  are respectively the Hamiltonians of atom 1 and atom 2 (taking  $\hbar = 1$ ):

$$\begin{aligned} \hat{H}_1 &= e^{-i\Delta_1 t} \Omega_{11} |1\rangle_1 \langle r| + \text{H.c.}, \\ \hat{H}_2 &= e^{-i\Delta_2 t} (\Omega_{21} |0\rangle_2 \langle r| + \Omega_{22} |1\rangle_2 \langle r|) + \text{H.c.}, \end{aligned} \quad (2)$$

and the third term in Eq. (1) describes the Rydberg interaction:

$$\hat{V}_{rr} = V |rr\rangle \langle rr|. \quad (3)$$

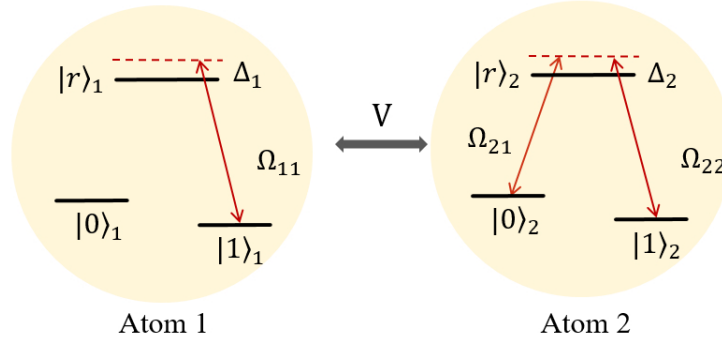


FIG. 1. Schematic diagram of three-level Rydberg atoms interacting with lasers.

In the two-atom basis, by applying the unitary operator  $\hat{U} = \exp[-i(\Delta_2 - \Delta_1)t|rr\rangle\langle rr|]$ , the system is shifted to the rotating frame, giving rise to

$$\begin{aligned} \hat{H}' &= \hat{U}^\dagger \hat{H} \hat{U} + i \frac{d\hat{U}^\dagger}{dt} \hat{U} \\ &= \left[ \Omega_{11} e^{-i\Delta_1 t} (|10\rangle \langle r0| + |11\rangle \langle r1|) + \Omega_{11} e^{i(\Delta_2 - 2\Delta_1)t} |1r\rangle \langle rr| \right. \\ &\quad + \Omega_{21} e^{-i\Delta_2 t} (|0r\rangle \langle 00| + |1r\rangle \langle 10|) + \Omega_{21} e^{-i\Delta_1 t} |rr\rangle \langle r0| \\ &\quad + \Omega_{22} e^{-i\Delta_2 t} (|0r\rangle \langle 01| + |1r\rangle \langle 11|) + \Omega_{22} e^{-i\Delta_1 t} |rr\rangle \langle r1| + \text{H.c.}] \\ &\quad + (V + \Delta_1 - \Delta_2) |rr\rangle \langle rr|. \end{aligned} \quad (4)$$

Under the conditions  $\Delta_1, \Delta_2 \gg \Omega_{11}, \Omega_{21}, \Omega_{22}$  and  $\Delta_2 \gg \Delta_1$ , we can obtain the effective Hamiltonian (see Appendix A)

$$\hat{H}_{\text{eff}} = (\Omega_1 |rr\rangle\langle 11| + \Omega_2 |rr\rangle\langle 10| + \text{H.c.}) + \delta |rr\rangle\langle rr|, \quad (5)$$

where

$$\begin{aligned} \Omega_1 &= -\frac{\Omega_{21}\Omega_{11}}{\Delta_1}, \Omega_2 = -\frac{\Omega_{22}\Omega_{11}}{\Delta_1}, \\ \delta &= V + \Delta_1 - \Delta_2 - \frac{\Omega_{21}^2 + \Omega_{22}^2}{\Delta_1} - \frac{\Omega_{11}^2}{\Delta_2 - 2\Delta_1}. \end{aligned} \quad (6)$$

Here, the Stark shift terms are omitted because they can be eliminated by using auxiliary pulses or levels. To realize the Rydberg antiblockade effect and resonantly couple the ground states  $|10\rangle$  and  $|11\rangle$  with the double Rydberg state  $|rr\rangle$ , it is necessary to set  $\delta = 0$ , which can be achieved by setting specific values of  $V$ .

To implement the geometric CU gate via Rydberg atoms, we set the driving field as  $\Omega_1 = \Omega_0 \sin \frac{\theta}{2} e^{i\varphi}$ ,  $\Omega_2 = -\Omega_0 \cos \frac{\theta}{2}$ . Accordingly, the Hamiltonian becomes

$$\hat{H}'_{\text{eff}} = \Omega_0 |rr\rangle\langle B| + \text{H.c.} \quad (7)$$

Here  $|B\rangle = \sin \frac{\theta}{2} e^{i\varphi} |10\rangle - \cos \frac{\theta}{2} |11\rangle$  is called bright state. The evolution of the effective Hamiltonian actually corresponds to Rabi oscillations between the bright state and the double Rydberg state  $|rr\rangle$ . This Hamiltonian also admits a dark eigenstate  $|D\rangle = \cos \frac{\theta}{2} |10\rangle + \sin \frac{\theta}{2} e^{-i\varphi} |11\rangle$  with a zero eigenvalue, which is decoupled from the dynamics.

Next, we will show how to construct a two-qubit gate through reverse engineering using the dynamics of NHQC+. The system's evolution under the effective Hamiltonian  $\hat{H}'_{\text{eff}}$  is governed by the time-dependent Schrödinger equation:

$$i \frac{\partial}{\partial t} |\psi(t)\rangle = \hat{H}'_{\text{eff}} |\psi(t)\rangle. \quad (8)$$

In the computational subspaces  $|rr\rangle$  and  $|B\rangle$ , by defining two time-dependent angles  $\alpha$  and  $\beta$ , the state can be parameterized as follows:

$$|\psi(t)\rangle = \cos \frac{\beta}{2} |rr\rangle + ie^{-i\alpha} \sin \frac{\beta}{2} |B\rangle. \quad (9)$$

Simultaneously, the orthogonal evolved state  $|\psi_{\perp}(t)\rangle$  also satisfy Eq. (8), thus it can be parameterized as

$$|\psi_{\perp}(t)\rangle = ie^{i\alpha} \sin \frac{\beta}{2} |rr\rangle + \cos \frac{\beta}{2} |B\rangle. \quad (10)$$

To derive the pulse constraint equation determined by  $\alpha$  and  $\beta$ , we first substitute  $\Omega_0$  in Eq. (7) with  $\Omega_0 = \Omega_R + i\Omega_I$ . Then, based on Eqs. (7)–(10), we can obtain

$$\begin{aligned} \Omega_R &= (\dot{\alpha} \sin \alpha \tan \beta - \dot{\beta} \cos \alpha) / 2, \\ \Omega_I &= (\dot{\alpha} \cos \alpha \tan \beta + \dot{\beta} \sin \alpha) / 2. \end{aligned} \quad (11)$$

Based on the above equation, a suitable set of  $\alpha$  and  $\beta$  can be chosen to implement the evolution of the quantum gate. To satisfy the cyclic evolution condition, it is also necessary to ensure the boundary condition  $\beta(0) = \beta(T)$  holds. To obtain a pure geometric phase, we adopt the setting method from Ref. [30] for  $\beta$  and  $\alpha$ :

$$\begin{aligned} \beta(t) &= \pi \sin^2(\pi t / T), \\ \alpha(t) &= -\gamma \varepsilon(t) + 4 \sin^3[\beta(t) / 3], \\ \varepsilon(t) &= \begin{cases} 0, & t \in [0, T/2], \\ 1, & t \in [T/2, T], \end{cases} \end{aligned} \quad (12)$$

such that upon evolving for one period  $T$ , the dynamic phase is zero and the total phase is  $\gamma$ . Therefore, the evolution operator in computational basis  $\{|00\rangle, |01\rangle, |10\rangle, |11\rangle\}$  can be written as:

$$\begin{aligned} \hat{U}(\gamma, \theta, \varphi) &= |00\rangle\langle 00| + |01\rangle\langle 01| + |D\rangle\langle D| + e^{i\gamma} |B\rangle\langle B| \\ &= |0\rangle\langle 0| \otimes \hat{I} + |1\rangle\langle 1| \otimes \hat{u}, \end{aligned} \quad (13)$$

where

$$\begin{aligned} \hat{u} &= e^{i\frac{\gamma}{2}} \begin{pmatrix} \cos \frac{\gamma}{2} - i \cos \theta \sin \frac{\gamma}{2} & -ie^{i\varphi} \sin \theta \sin \frac{\gamma}{2} \\ -ie^{-i\varphi} \sin \theta \sin \frac{\gamma}{2} & \cos \frac{\gamma}{2} + i \cos \theta \sin \frac{\gamma}{2} \end{pmatrix} \\ &= e^{i\frac{\gamma}{2}} e^{-i\frac{\gamma}{2} \mathbf{n} \cdot \boldsymbol{\sigma}}. \end{aligned} \quad (14)$$

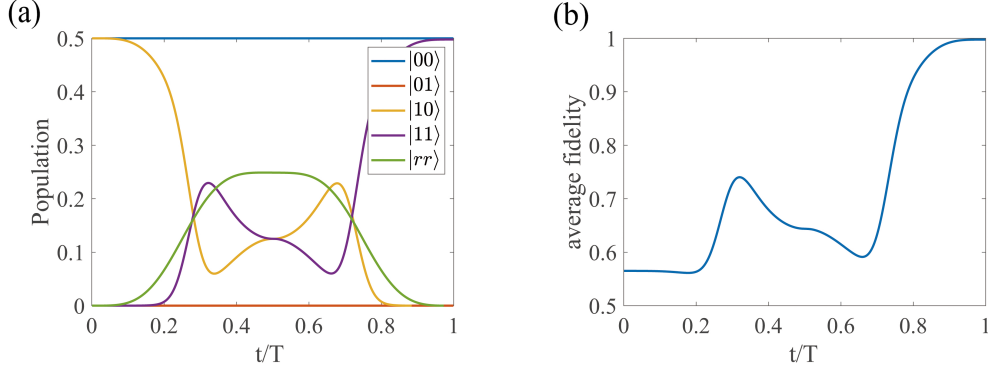


FIG. 2. (a) The population dynamics in the evolution of the CNOT gate. (b) The average fidelity of the CNOT gate changes over time, and the final average fidelity obtained is 0.9975.

Here,  $\sigma = (\sigma_x, \sigma_y, \sigma_z)$  denotes the standard Pauli matrices,  $\mathbf{n} = (\sin \theta \cos \varphi, -\sin \theta \sin \varphi, \cos \theta)$  denotes a unit vector. The parameters  $\beta$  and  $\varphi$  are adjusted independently to implement an arbitrary two-qubit NHQC+ controlled gate, in which  $\hat{u}$  represents any single-qubit operation, and we can implement a CU gate by adjusting the values of the laser parameters  $\gamma$ ,  $\theta$  and  $\varphi$ . For instance, we choose  $\gamma = \pi$ ,  $\theta = \frac{\pi}{2}$ ,  $\varphi = 0$  for the CNOT gate;  $\gamma = \pi$ ,  $\theta = 0$ ,  $\varphi = 0$  for the CZ gate; and  $\gamma = \frac{\pi}{2}$ ,  $\theta = \frac{\pi}{4}$ ,  $\varphi = 0$  for the CH gate.

### B. Robustness against spontaneous emission and laser intensity errors

Next, we will use numerical simulation to verify the feasibility of the logic gate scheme. In the ideal case, for a given initial state  $|\psi(0)\rangle$ , a quantum logic gate  $U$  can precisely evolve the state into the target state:

$$|\psi_{\text{ideal}}\rangle = U|\psi(0)\rangle. \quad (15)$$

However, in an open quantum system, the evolution is inevitably affected by noise, decoherence, and other environmental factors, causing the actual output state, described by the density matrix  $\rho$ , to deviate from the ideal case. In this case, the fidelity of the quantum state is defined as:

$$F = \langle \psi_{\text{ideal}} | \rho_{\text{actual}} | \psi_{\text{ideal}} \rangle. \quad (16)$$

The dynamical evolution of an open system is controlled by the Lindblad master equation,

$$\dot{\rho}(t) = i[\rho(t), H(t)] + \sum_j \sum_k \left[ L_j^k \rho L_j^{k\dagger} - \frac{1}{2} \left( L_j^{k\dagger} L_j^k \rho + \rho L_j^{k\dagger} L_j^k \right) \right], \quad (17)$$

where  $H(t)$  represents the total Hamiltonian of the system, and  $\rho(t)$  denotes the density matrix of the system state. For Rydberg atoms, the spontaneous decay of Rydberg states constitutes the primary factor affecting system fidelity, described by Lindblad operators  $L_j^k = \sqrt{\Gamma/2}|k\rangle_j \langle r|$ , where  $k = 0, 1$  denotes an arbitrary initial state,  $j$  is the atom index, and  $\Gamma$  is the decay rate from the Rydberg state to the ground state.

In our scheme, we need to select an appropriate detuning to satisfy the prerequisite conditions of the effective Hamiltonian. This affects the Rabi frequency of the laser, the gate evolution time, and the interaction strength between Rydberg atoms. Specifically, shorter gate evolution times lead to higher gate fidelity, but this requires larger Rabi frequencies, which in turn result in greater detuning and stronger Rydberg interaction strengths. Next we use the CNOT gate as an example to illustrate parameter selection in our scheme. For the Rabi frequency of the laser, we adopted a typical experimental value of  $\Omega_{11} = 2\pi \times 4.5$  MHz and  $\Omega_{21} = \Omega_{22} = 2\pi \times 14$  MHz, with corresponding detunings of  $\Delta_1 = 2\pi \times 50$  MHz and  $\Delta_2 = 2\pi \times 300$  MHz, respectively. The Rydberg interaction strength is  $V = 2\pi \times 306$  MHz. In this paper, we assume the Rydberg atoms to be  $^{87}\text{Rb}$  atoms, with the Rydberg state set as  $|70S_{1/2}\rangle$ . According to Ref. [33], at 0K, the lifetime  $\tau$  of the Rydberg state is 416  $\mu\text{s}$ , and the decay rate  $\Gamma = 1/\tau \approx 2.4$  kHz. Under these parameters, the gate operation time is 5.5  $\mu\text{s}$  with a fidelity of 0.9977, if the initial state is  $|\psi(0)\rangle = \frac{1}{\sqrt{2}}(|00\rangle + |10\rangle)$ .

To examine performance for different initial states, we calculate the average fidelity expressed as

$$F = \frac{1}{(2\pi)^2} \int_0^{2\pi} \int_0^{2\pi} \langle \psi | \rho(t) | \psi \rangle d\alpha d\beta, \quad (18)$$

where  $\alpha$  and  $\beta$  are arbitrary coefficients in the general initial state  $|\psi(0)\rangle = (\cos \alpha|0\rangle_1 + \sin \alpha|1\rangle_1) \otimes (\cos \beta|0\rangle_2 + \sin \beta|1\rangle_2)$ . In Fig. 2, we separately show the time evolution of the average fidelity, as well as the changes in the populations of each state when the initial state is  $|\psi(0)\rangle = \frac{1}{\sqrt{2}}(|00\rangle + |10\rangle)$ , which shows that our scheme possesses sufficient robustness. In addition, due to the instability of the laser, the Rabi frequency may admit certain errors. We consider the driving pulses  $\Omega_1$  and  $\Omega_2$  varying within the ranges  $(1 + \epsilon_1)\Omega_1$  and  $(1 + \epsilon_2)\Omega_2$ , respectively, where the error fractions  $\epsilon_1, \epsilon_2 \in [-0.1, 0.1]$ . In Fig.3(a), we plot the fidelity variation caused by laser errors. Fig.3(b) shows the fidelity under different decay rates, with  $\Gamma$  ranging from 0.2 to 5 kHz. Overall, the fidelity under parameter fluctuations demonstrates that our scheme is indeed robust.

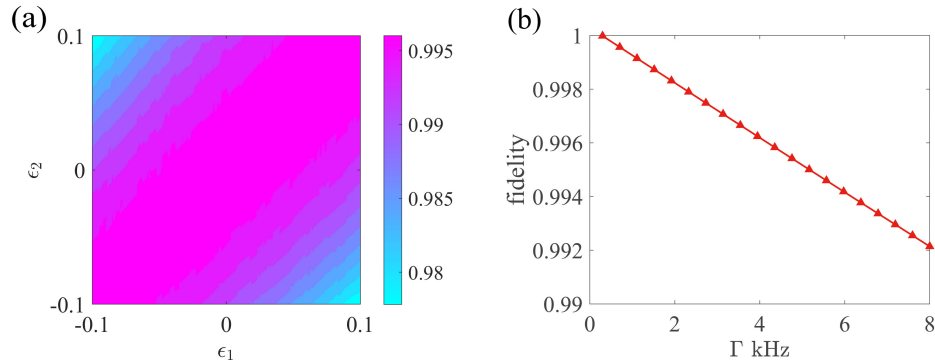


FIG. 3. (a) Schematic diagram of fidelity under laser error. (b) Fidelity under different decay rates.

### III. NON-LOCAL CU GATE PROTOCOL

Quantum entanglement constitutes a fundamental resource in quantum computing, which necessitates the development of reliable quantum gates to facilitate operations on entangled atomic systems. Nevertheless, many quantum computing architectures demand long-distance entanglement between qubits. In these scenarios, conventional Rydberg-mediated quantum gates are inapplicable, as they impose stringent constraints on the spatial proximity of the atoms. Although optical tweezers can be used to move atoms in Rydberg arrays, atom transport increases susceptibility to decoherence [34]. Therefore, the construction of non-local quantum gates is essential.

The primary approach for constructing non-local quantum gates relies on teleportation techniques. Over the past few decades, researchers have proposed several schemes for implementing non-local CNOT gates [35–38]. Following the fundamental ideas of these proposals, we extend the previously introduced NHQC+ CU gate into a non-local CU gate by adapting the Bell-state-based teleportation technique.

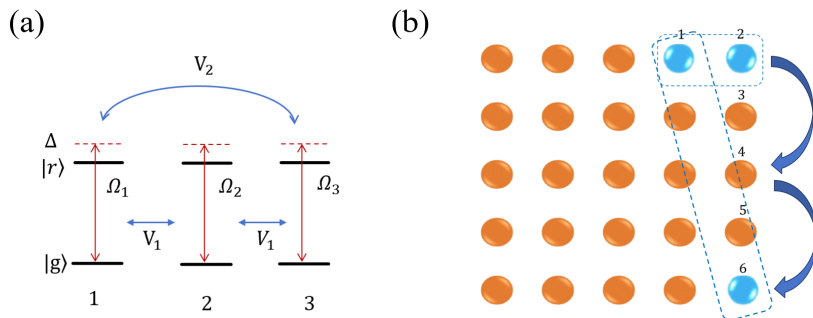


FIG. 4. (a) Schematics of interaction between three Rydberg atoms and lasers. (b) Diagram illustrating the process of entanglement transfer.

In non-local quantum gates, the entanglement channel should also be long-range. Wu et al. [39] proposed a technique for Bell state transfer utilizing the anti-blockade effect. Applying this technique to non-local quantum gate protocols can enhance the flexibility of our scheme. Considering a three-atom two-level system of Rydberg atoms as shown in

Fig. 4(a), the Hamiltonian under laser excitation can be written as

$$\begin{aligned}\hat{H}_s &= \hat{H}_0 + \hat{H}_{dd}, \\ \hat{H}_0 &= (\Omega_1|g\rangle_1\langle r|e^{i\Delta t} + \Omega_2|g\rangle_2\langle r|e^{i\Delta t} + \Omega_3|g\rangle_3\langle r|e^{i\Delta t}) + \text{H.c.}, \\ \hat{H}_{dd} &= V_1|rrg\rangle\langle rrg| + V_1|grr\rangle\langle grr| + V_2|rgr\rangle\langle rgr| + (2V_1 + V_2)|rrr\rangle\langle rrr|,\end{aligned}\quad (19)$$

where  $H_0$  is the Hamiltonian of the free atoms,  $H_{dd}$  is the Hamiltonian of the interatomic interactions, and  $V_1$  and  $V_2$  represent the dipole-dipole interactions between nearest-neighbor and next-nearest-neighbor atoms, respectively. By applying a unitary transformation with the operator  $U = e^{-iH_{dd}t}$  to rotate the Hamiltonian, and under the condition  $\Delta = V_1$ ,  $V_{1,2} \gg \Omega_{1,2,3}$ , an anti-blockade three-atom Hamiltonian is ultimately obtained,

$$\begin{aligned}\hat{H} &= J_1|rgg\rangle\langle rrg| + J_2|rrg\rangle\langle grg| + \\ &J_3|grg\rangle\langle grr| + J_1|grr\rangle\langle ggr| + \text{H.c.},\end{aligned}\quad (20)$$

To achieve perfect entanglement transfer, the parameters  $J_i$  in the above equation must satisfy the following relation:

$$J_i = \sqrt{i(N-i)\Omega}. \quad (21)$$

Where  $N$  is the atomic serial number to which the entanglement needs to be transferred. Next, we demonstrate the transfer of entanglement from adjacent atoms 1 and 2 to atoms 1 and 6 (as shown in Fig. 4(b)). First, the six atoms are prepared in the following state:

$$|\psi(t=0)\rangle = \frac{|gr\rangle_{12} + |rg\rangle_{12}}{\sqrt{2}} \otimes |gggg\rangle_{3456}. \quad (22)$$

Next, three laser beams with Rabi frequencies satisfying Eq. (21) are applied to atoms 2, 3, and 4, respectively. When the evolution time reaches  $t = \pi/\Omega$ , we find that the entire system evolves to

$$|\psi(t = \frac{\pi}{\Omega})\rangle = \frac{|gr\rangle_{14} + |rg\rangle_{14}}{\sqrt{2}} \otimes |gggg\rangle_{2356}. \quad (23)$$

This process enables the transfer of the Bell state from atoms 1 and 2 to atoms 1 and 4. When the laser satisfying Eq. (21) are applied to atoms 4, 5, and 6, respectively, and after another evolution period of  $t = \pi/\Omega$ , the final state of the entire system is calculated to be

$$|\psi(t = \frac{2\pi}{\Omega})\rangle = \frac{|gr\rangle_{16} + |rg\rangle_{16}}{\sqrt{2}} \otimes |gggg\rangle_{2345}. \quad (24)$$

In this way, entanglement is successfully transferred from atoms 1 and 2 to atoms 1 and 6. This process can be repeated to propagate the entanglement even further. Ref. [39] quantifies the maximum number of such steps achievable with specific experimental parameters, proving that this approach is viable for large-scale quantum information transfer within the lifetime of the Rydberg state.

In our proposed scheme, we improve upon the teleportation protocol of Wu et al [40]. Once the entanglement is prepared (the preparation method can follow that in Ref. [40]) and transferred to the designated locations, we assume the control qubit carries information  $\alpha|0\rangle + \beta|1\rangle$  and is labeled as atom 1, while the target qubit is  $\delta|0\rangle + \gamma|1\rangle$  and labeled as atom 4. The two entangled atoms are labeled as atoms 2 and 3. Furthermore, it is required that atom 2 is within the Rydberg interaction radius of atom 1, and atom 3 is within the Rydberg interaction radius of atom 4. Under these conditions, the state of the entire system is

$$(\alpha|0\rangle + \beta|1\rangle)_1 \otimes \left(\frac{1}{\sqrt{2}}|r1\rangle + |1r\rangle\right)_{23} \otimes (\delta|0\rangle + \gamma|1\rangle)_4. \quad (25)$$

Additionally, we need to define the following Bell states:

$$\begin{cases} |\Phi_{\pm}^{1,2}\rangle = \frac{1}{\sqrt{2}}(|0\rangle_1|1\rangle_2 \pm |1\rangle_1|r\rangle_2), \\ |\Psi_{\pm}^{1,2}\rangle = \frac{1}{\sqrt{2}}(|0\rangle_1|r\rangle_2 \pm |1\rangle_1|1\rangle_2). \end{cases} \quad (26)$$

Then, Eq. (25) can be rewritten as

$$\begin{aligned} &\frac{1}{2} \left[ |\Phi_+^{1,2}\rangle (\alpha|r\rangle_3 + \beta|1\rangle_3) + |\Phi_-^{1,2}\rangle (\alpha|r\rangle_3 - \beta|1\rangle_3) \right. \\ &\quad \left. + |\Psi_+^{1,2}\rangle (\alpha|1\rangle_3 + \beta|r\rangle_3) + |\Psi_-^{1,2}\rangle (\alpha|1\rangle_3 - \beta|r\rangle_3) \right]. \end{aligned} \quad (27)$$

TABLE I. The relationship between the recovery operation and the joint measurement.  $M$  denotes the outcome of the joint measurement,  $U_M$  represents the corresponding recovery operation, and “State” denotes the quantum state of atom 3 after the action of the Hamiltonian from Eq. (31).

$M$	State	$U_m$
$ 1r\rangle$	$\alpha 0\rangle + \beta 1\rangle$	$I$
$ 11\rangle$	$\alpha 0\rangle - \beta 1\rangle$	$Z$
$ 0r\rangle$	$\alpha 1\rangle + \beta 0\rangle$	$X$
$ 01\rangle$	$\alpha 1\rangle - \beta 0\rangle$	$XZ$

Therefore, a Bell basis measurement can be performed on atoms 1 and 2. First, the Bell states will be disentangled. Here, the CNOT gate we constructed can be directly applied, with the control and target atoms being atom 2 and atom 1, respectively. Thus, Eq. (26) becomes

$$\begin{cases} |\Phi_{\pm}^{1,2}\rangle \rightarrow \frac{1}{\sqrt{2}}|1\rangle_1 (|1\rangle_2 \pm |r\rangle_2), \\ |\Psi_{\pm}^{1,2}\rangle \rightarrow \frac{1}{\sqrt{2}}|0\rangle_1 (|r\rangle_2 \pm |1\rangle_2). \end{cases} \quad (28)$$

Then, apply a  $\pi/2$  pulse to atom 3 that realizes the transformation  $\frac{1}{\sqrt{2}}|1\rangle + |r\rangle \rightarrow |1\rangle$ ,  $\frac{1}{\sqrt{2}}|1\rangle - |r\rangle \rightarrow |r\rangle$ . The Bell states then become

$$|\Phi_{\pm}^{1,2}\rangle \rightarrow \begin{cases} |1\rangle_1 |r\rangle_2 \\ |1\rangle_1 |1\rangle_2, \end{cases} \quad (29)$$

$$|\Psi_{\pm}^{1,2}\rangle \rightarrow \begin{cases} |0\rangle_1 |r\rangle_2 \\ |0\rangle_1 |1\rangle_2. \end{cases} \quad (30)$$

Finally, performing a joint measurement on atoms 1 and 2 completes the Bell basis measurement. To realize the CU gate, we still need to apply the following Hamiltonian to atom 3:

$$\hat{H} = (\Omega_{1r}|r\rangle\langle 0| + \text{H.c.}) + V|rr\rangle\langle rr|. \quad (31)$$

Then, based on the measurement results of the Bell basis, the corresponding recovery operations are performed (see Table 1). The control bit information of the non-local CU gate is perfectly transferred to atom 3. Subsequently, by executing a local CU operation with atom 3 as the control bit and atom 4 as the target bit, the implementation of the non-local CU gate is completed.

#### IV. APPLICATION — 4-QUBIT ENTANGLED STATE TRANSFORMATION

In the field of quantum information processing, different types of entangled states play distinct roles, and the transformation between entangled states can further enhance the efficiency of quantum computing. Recent theoretical breakthroughs have been achieved in three-qubit implementations using Rydberg atom arrays [41–43]. However, these schemes rely on designing specific Hamiltonians and impose strict requirements on the spatial arrangement and distances of the three atoms, which significantly limit their applicability. Moreover, extending these schemes to a larger number of qubits is challenging, as it requires extensive computational resources to derive feasible effective Hamiltonians.

As a highly entangled resource, cluster states possess exceptional robustness and persistence, making them promising candidates for a wide range of quantum tasks [44]. However, a cluster state requires at least four qubits to form. To date, the mutual transformation between cluster states and other four-qubit entangled states remains largely unexplored. In this paper, we demonstrate that such transformations can be systematically and efficiently realized using our proposed quantum gates. Before introducing the quantum circuit we designed for entangled state conversion, we first present the basic forms of the employed four-qubit entangled states:

$$\begin{aligned} |GHZ\rangle &= \frac{1}{\sqrt{2}}(|0000\rangle + |1111\rangle), \\ |\text{cluster}\rangle &= \frac{1}{2}(|0000\rangle + |1100\rangle + |0011\rangle - |1111\rangle), \\ |W\rangle &= \frac{1}{2}(|0001\rangle + |0010\rangle + |0100\rangle + |1000\rangle). \end{aligned} \quad (32)$$

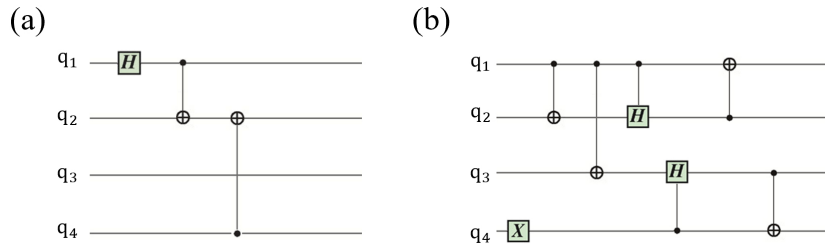


FIG. 5. Quantum circuits for entanglement conversion: (a)  $GHZ$  to cluster state, (b)  $GHZ$  to  $W$  state.  $q_i$  ( $i = 1, 2, 3, 4$ ) denotes the qubit index.

The conversion from a 4-qubit  $GHZ$  state to a cluster state requires only one single-qubit Hadamard gate and two CNOT gates. Fig. 5(a) illustrates one possible scheme, as the position of the single-qubit Hadamard operation in the first step can be chosen arbitrarily. To revert from the cluster state back to the  $GHZ$  state, one simply needs to apply the inverse of this circuit. For the conversion from a 4-qubit  $GHZ$  state to a  $W$  state, the quantum circuit is shown in Fig. 5(b). The process begins with the application of a single-qubit  $X$  gate, followed by two CNOT gates, then two CH gates, and finally two more CNOT gates. Similarly, this circuit is not unique—the position of the  $X$  gate can be changed, which in turn alters the control and target qubits of the subsequent controlled gates. For the conversion from the  $W$  state to the cluster state, using only single-qubit gates and two-qubit gates is difficult. It requires introducing an additional ancilla qubit and performing a measurement on it. The circuit before measurement is shown in Fig. 6(a), and depending on the measurement outcome, the gate operations in Fig. 6(b) or Fig. 6(c) are subsequently executed. The two-qubit gates in the scheme can be replaced with non-local gates as needed.

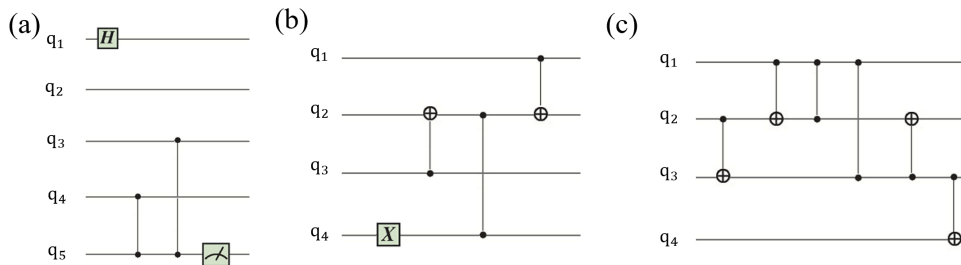


FIG. 6. (a) The entanglement conversion circuit from  $W$  state to cluster state before measurement. Qubit  $q_5$  is the ancilla, which is measured in the  $X$ -basis. (b) Feed-forward circuit for ancilla qubit measurement result 1. (c) Feed-forward circuit for ancilla qubit measurement result 0.

## V. CONCLUSION

In summary, we have proposed a robust and flexible scheme for constructing arbitrary two-qubit controlled gates by combining non-adiabatic holonomic quantum computation with the Rydberg anti-blockade effect. Through reverse-engineering of pulse design based on the dynamical invariant method, geometric non-adiabatic quantum gate operations are realized under specific large-detuning conditions, demonstrating strong robustness against local noise. We further extend the scheme to nonlocal gates through entanglement transfer and quantum teleportation. Based on the implemented CU gates, We have systematically proposed a protocol for the mutual conversion between four-qubit  $GHZ$  states and cluster states, as well as between  $GHZ$  states and  $W$  states. These protocols require only basic quantum gate operations, thereby avoiding the design of complex many-body Hamiltonians and significantly enhancing the flexibility and operability of entanglement resource management. This study not only extends the application of geometric quantum computation in Rydberg atom platforms but also provides valuable insights for advancing large-scale quantum information processing.

## ACKNOWLEDGMENTS

This work was supported by the National Natural Science Foundation of China (12522413, 12474493); Natural Science Foundation of Zhejiang Province, China (LR22A040001, LY21A040004).

### Appendix A: DERIVATION OF THE EFFECTIVE HAMILTONIAN

In this appendix, we demonstrate the derivation of Eqs. (5) and (6). First, we rewrite Eq. (4) into two parts:

$$\hat{H}' = \hat{H}_0 + \hat{H}_I, \quad (\text{A1})$$

where

$$\begin{aligned} \hat{H}_0 = & \Omega_{11}e^{-i\Delta_1 t}(|10\rangle\langle r0| + |11\rangle\langle r1|) \\ & + \Omega_{21}e^{-i\Delta_2 t}(|0r\rangle\langle 00| + |1r\rangle\langle 10|) \\ & + \Omega_{22}e^{-i\Delta_2 t}(|0r\rangle\langle 01| + |1r\rangle\langle 11|) \\ & + \Omega_{21}e^{-i\Delta_1 t}|rr\rangle\langle r0| + \Omega_{22}e^{-i\Delta_1 t}|rr\rangle\langle r1| \\ & + \Omega_{11}e^{i(\Delta_2 - 2\Delta_1)t}|1r\rangle\langle rr| + \text{H.c.}, \end{aligned} \quad (\text{A2})$$

and

$$\hat{H}_I = (V + \Delta_1 - \Delta_2)|rr\rangle\langle rr|. \quad (\text{A3})$$

According to the effective Hamiltonian theory, the Hamiltonian of  $\hat{H}_0$  is written in the following form:

$$\hat{H}_0 = \sum_{n=1,2,3} \hat{h}_n^\dagger e^{i\Delta_n t} + \hat{h}_n e^{-i\Delta_n t}, \quad (\text{A4})$$

in which  $\hat{h}_1$ ,  $\hat{h}_2$ , and  $\hat{h}_3$  are of the following forms:

$$\begin{aligned} \hat{h}_1 = & \Omega_{11}(|10\rangle\langle r0| + |11\rangle\langle r1|) + \Omega_{21}|rr\rangle\langle r0| + \Omega_{22}|rr\rangle\langle r1|, \\ \hat{h}_2 = & \Omega_{21}(|0r\rangle\langle 00| + |1r\rangle\langle 10|) + \Omega_{22}(|0r\rangle\langle 01| + |1r\rangle\langle 11|), \\ \hat{h}_3 = & \Omega_{11}|1r\rangle\langle rr|. \end{aligned} \quad (\text{A5})$$

After removing the high-frequency oscillation terms,  $\hat{H}_0$  becomes a simplified form:

$$\hat{H}_{0,\text{eff}} = \frac{1}{\Delta_1} [\hat{h}_1^\dagger, \hat{h}_1] + \frac{1}{\Delta_2} [\hat{h}_2^\dagger, \hat{h}_2] + \frac{1}{\Delta_2 - 2\Delta_1} [\hat{h}_3^\dagger, \hat{h}_3]. \quad (\text{A6})$$

By inserting Eq. (A5) into (A6) the effective Hamiltonian can be changed to

$$\begin{aligned} \hat{H}_{\text{eff}} = & \left[ \frac{\Omega_{21}^2}{\Delta_2} |00\rangle\langle 00| + \left( \frac{\Omega_{22}^2}{\Delta_2} - \frac{\Omega_{11}^2}{\Delta_1} \right) |11\rangle\langle 11| + \frac{\Omega_{22}^2}{\Delta_2} |01\rangle\langle 01| + \left( \frac{\Omega_{21}^2}{\Delta_2} - \frac{\Omega_{11}^2}{\Delta_1} \right) |10\rangle\langle 10| \right. \\ & + \frac{\Omega_{11}^2 + \Omega_{21}^2}{\Delta_1} (|r0\rangle\langle r0| + |r1\rangle\langle r1|) - \frac{\Omega_{21}^2 + \Omega_{22}^2}{\Delta_2} (|0r\rangle\langle 0r| + |1r\rangle\langle 1r|) - \frac{\Omega_{21}\Omega_{11}}{\Delta_1} |rr\rangle\langle 10| \\ & \left. - \frac{\Omega_{22}\Omega_{11}}{\Delta_1} |rr\rangle\langle 11| + \frac{\Omega_{22} + \Omega_{21}}{\Delta_2} (|01\rangle\langle 00| + |11\rangle\langle 10|) + \text{H.c.} \right] \\ & + \left( V + \Delta_1 - \Delta_2 - \frac{\Omega_{21}^2 + \Omega_{22}^2}{\Delta_1} - \frac{\Omega_{11}^2}{\Delta_2 - 2\Delta_1} \right) |rr\rangle\langle rr|. \end{aligned} \quad (\text{A7})$$

---

[1] C. Monroe, Quantum information processing with atoms and photons, *Nature* **416**, 238 (2002).

[2] P. W. Shor, Polynomial-time algorithms for prime factorization and discrete logarithms on a quantum computer, *SIAM review* **41**, 303 (1999).

- [3] L. K. Grover, Quantum mechanics helps in searching for a needle in a haystack, *Physical Review Letters* **79**, 325 (1997).
- [4] A. D. King, A. Nocera, M. M. Rams, J. Dziarmaga, R. Wiersema, W. Bernoudy, J. Raymond, N. Kaushal, N. Heinsdorf, R. Harris, *et al.*, Beyond-classical computation in quantum simulation, *Science* **388**, 199 (2025).
- [5] M. Benedetti, H. Buhrman, and J. Weggemans, Provable and verifiable quantum advantage in sample complexity, *Physical Review Letters* **136**, 040601 (2026).
- [6] F. Wilczek and A. Zee, Appearance of gauge structure in simple dynamical systems, *Physical Review Letters* **52**, 2111 (1984).
- [7] P. Zanardi and M. Rasetti, Holonomic quantum computation, *Physics Letters A* **264**, 94 (1999).
- [8] W. Niu, J.-L. Wu, P. Wang, and X. Ji, Error-insensitive 3d entanglement gate with optimal control of geometric evolution, *Annalen der Physik* **533**, 2100145 (2021).
- [9] J. Zhang, T. H. Kyaw, S. Filipp, L.-C. Kwek, E. Sjöqvist, and D. Tong, Geometric and holonomic quantum computation, *Physics Reports* **1027**, 1 (2023).
- [10] O. Sönnernborn, Estimate of the time required to perform a nonadiabatic holonomic quantum computation, *Physical Review A* **109**, 062433 (2024).
- [11] V. Neef, J. Pinske, T. A. Wolterink, K. Becker, M. Heinrich, S. Scheel, and A. Szameit, Non-adiabatic holonomies for photonic quantum computing, *Optica Quantum* **3**, 93 (2025).
- [12] G. Xu, P. Zhao, T. Xing, E. Sjöqvist, and D. Tong, Composite nonadiabatic holonomic quantum computation, *Physical Review A* **95**, 032311 (2017).
- [13] P. Zhao, X. Wu, T. Xing, G. Xu, and D. Tong, Nonadiabatic holonomic quantum computation with rydberg superatoms, *Physical Review A* **98**, 032313 (2018).
- [14] Y. Liang and Z.-Y. Xue, Nonadiabatic geometric quantum gates with on-demand trajectories, *Physical Review Applied* **21**, 064048 (2024).
- [15] J.-L. Wu, Y. Wang, J.-X. Han, S.-L. Su, Y. Xia, Y. Jiang, and J. Song, Unselective ground-state blockade of rydberg atoms for implementing quantum gates, *Frontiers of Physics* **17**, 22501 (2022).
- [16] S. Li, T. Chen, and Z.-Y. Xue, Fast holonomic quantum computation on superconducting circuits with optimal control, *Advanced Quantum Technologies* **3**, 2000001 (2020).
- [17] C. Zu, W.-B. Wang, L. He, W.-G. Zhang, C.-Y. Dai, F. Wang, and L.-M. Duan, Experimental realization of universal geometric quantum gates with solid-state spins, *Nature* **514**, 72 (2014).
- [18] S.-L. Zhu and Z. Wang, Implementation of universal quantum gates based on nonadiabatic geometric phases, *Physical Review Letters* **89**, 097902 (2002).
- [19] S. Li, P. Shen, T. Chen, and Z.-Y. Xue, Noncyclic nonadiabatic holonomic quantum gates via shortcuts to adiabaticity, *Frontiers of Physics* **16**, 51502 (2021).
- [20] F.-Q. Guo, J.-L. Wu, X.-Y. Zhu, Z. Jin, Y. Zeng, S. Zhang, L.-L. Yan, M. Feng, and S.-L. Su, Complete and nondestructive distinguishment of many-body rydberg entanglement via robust geometric quantum operations, *Physical Review A* **102**, 062410 (2020).
- [21] F.-Q. Guo, X.-Y. Zhu, M.-R. Yun, L.-L. Yan, Y. Zhang, Y. Jia, and S.-L. Su, Multiple-qubit nonadiabatic noncyclic geometric quantum computation in rydberg atoms, *Europhysics Letters* **137**, 55001 (2022).
- [22] B.-J. Liu, X.-K. Song, Z.-Y. Xue, X. Wang, and M.-H. Yung, Plug-and-play approach to nonadiabatic geometric quantum gates, *Physical Review Letters* **123**, 100501 (2019).
- [23] M. Morgado and S. Whitlock, Quantum simulation and computing with rydberg-interacting qubits, *AVS Quantum Science* **3** (2021).
- [24] I. Beterov, D. Tretyakov, V. Entin, E. Yakshina, I. Ryabtsev, M. Saffman, and S. Bergamini, Application of adiabatic passage in rydberg atomic ensembles for quantum information processing, *Journal of Physics B: Atomic, Molecular and Optical Physics* **53**, 182001 (2020).
- [25] M. Li, F.-Q. Guo, Z. Jin, L.-L. Yan, E.-J. Liang, and S.-L. Su, Multiple-qubit controlled unitary quantum gate for rydberg atoms using shortcut to adiabaticity and optimized geometric quantum operations, *Physical Review A* **103**, 062607 (2021).
- [26] C.-Y. Guo, L.-L. Yan, S. Zhang, S.-L. Su, and W. Li, Optimized geometric quantum computation with a mesoscopic ensemble of rydberg atoms, *Physical Review A* **102**, 042607 (2020).
- [27] Y. Liang, X.-D. Tian, L.-N. Ji, and Z.-Y. Xue, Error-resilient geometric entangling gates in rydberg atoms, *Physical Review Applied* **24**, 034025 (2025).
- [28] Y. Ming, Z.-X. Fu, and Y.-X. Du, Geometric gates in atomic arrays without rydberg blockade, *Physical Review A* **112**, 042609 (2025).
- [29] S.-L. Su, Y. Gao, E. Liang, and S. Zhang, Fast rydberg antiblockade regime and its applications in quantum logic gates, *Physical Review A* **95**, 022319 (2017).
- [30] Y. Xiao, Y.-H. Kang, R.-H. Zheng, J. Song, Y.-H. Chen, and Y. Xia, Effective nonadiabatic holonomic swap gate with rydberg atoms using invariant-based reverse engineering, *Physical Review A* **109**, 062610 (2024).
- [31] W.-X. Li, J.-L. Wu, S.-L. Su, and J. Qian, High-tolerance antiblockade swap gates using optimal pulse drivings, *Physical Review A* **109**, 012608 (2024).
- [32] J.-L. Wu, Y. Wang, J.-X. Han, Y.-K. Feng, S.-L. Su, Y. Xia, Y. Jiang, and J. Song, One-step implementation of rydberg-antiblockade swap and controlled-swap gates with modified robustness, *Photonics Research* **9**, 814 (2021).
- [33] I. Beterov, I. Ryabtsev, D. Tretyakov, and V. Entin, Quasiclassical calculations of blackbody-radiation-induced depopulation rates and effective lifetimes of rydberg  $n s$ ,  $n p$ , and  $n d$  alkali-metal atoms with  $n = 80$ , *Physical Review A* **79**, 052504 (2009).
- [34] N. Berthussen, D. Devulapalli, E. Schoute, A. M. Childs, M. J. Gullans, A. V. Gorshkov, and D. Gottesman, Toward a 2d

- local implementation of quantum low-density parity-check codes, *PRX Quantum* **6**, 010306 (2025).
- [35] Y.-H. Han, C. Cao, L. Fan, and R. Zhang, Scheme for implementing nonlocal high-fidelity quantum controlled-not gates on quantum-dot-confined electron spins using optical microcavities and photonic hyperentanglement, *Frontiers in Physics* **10**, 1006255 (2022).
  - [36] A.-P. Liu, L.-Y. Cheng, Q. Guo, S.-L. Su, H.-F. Wang, and S. Zhang, Heralded teleportation of a controlled-not gate for nitrogen-vacancy centers coupled to a microtoroid resonator, *Laser Physics* **29**, 025205 (2019).
  - [37] D. Gottesman and I. L. Chuang, Demonstrating the viability of universal quantum computation using teleportation and single-qubit operations, *Nature* **402**, 390 (1999).
  - [38] Y.-F. Huang, X.-F. Ren, Y.-S. Zhang, L.-M. Duan, and G.-C. Guo, Experimental teleportation of a quantum controlled-not gate, *Physical Review Letters* **93**, 240501 (2004).
  - [39] Y. Wu, Y. Jiao, B. Guan, F. Mei, L. Xiao, and S. Jia, Perfect quantum state transfer in neutral atoms based on rydberg anti-blockade, *Journal of Quantum Optics* **31**, 020301 (2025).
  - [40] H. Wu, Z.-B. Yang, L.-T. Shen, and S.-B. Zheng, Quantum teleportation and computation with rydberg atoms in an optical lattice, *Journal of Physics B: Atomic, Molecular and Optical Physics* **46**, 185502 (2013).
  - [41] X. Shao, F. Liu, X. Xue, W. Mu, and W. Li, High-fidelity interconversion between greenberger-horne-zeilinger and w states through floquet-lindblad engineering in rydberg atom arrays, *Physical Review Applied* **20**, 014014 (2023).
  - [42] T. Haase, G. Alber, and V. M. Stojanović, Conversion from w to greenberger-horne-zeilinger states in the rydberg-blockade regime of neutral-atom systems: Dynamical-symmetry-based approach, *Physical Review A* **103**, 032427 (2021).
  - [43] J. Wang, Y. Ji, L. Yang, C. Wang, L. Dong, and X. Xiu, Deterministic interconversion of ghz state and klm state via lie-transform-based pulse design in rydberg atoms, *Communications in Theoretical Physics* **77**, 065103 (2025).
  - [44] L.-J. Yu, Z.-L. Zhao, Z.-Q. Yuan, Z. Zhao, L. Dong, and X.-M. Xiu, Generation of five-photon hyperentangled cluster state with three-photon ghz state and bell state via weak cross-kerr nonlinearity., *Quantum Information Processing* **23** (2024).